Title

Facile incorporation of technetium into magnetite, magnesioferrite, and hematite by formation of ferrous nitrate in situ : precursors to iron oxide nuclear waste forms

Journal

Dalton Transactions, 47(30)

ISSN

1477-9226

Authors

Lukens, Wayne W

Saslow, Sarah A

Publication Date

2018-07-31

DOI

10.1039/c8dt01356j

Peer reviewed

Facile incorporation of technetium into magnetite, magnesioferrite, and hematite by formation of ferrous nitrate *in situ*: precursors to iron oxide nuclear waste forms

Wayne W. Lukens*[a] and Sarah A. Saslow [b]

Abstract

The fission product, ^{99}Tc, presents significant challenges to the long-term disposal of nuclear waste to its long half-life, high fission yield, and to the environmental mobility of pertechnetate (TcO_4^-), the stable Tc species in aerobic environments. Migration of ^{99}Tc from disposal sites can potentially be prevented by incorporating it into durable waste forms based on environmentally stable minerals. Since Tc(IV) and Fe(III) have the same ionic radius, Tc(IV) can replace Fe(III) in iron oxides. Environmentally durable iron oxides include goethite (α-FeOOH), hematite (α-Fe_2O_3), and magnesioferrite ($MgFe_2O_4$). The incorporation of Tc into two of these, hematite and magnesioferrite, as well as magnetite (Fe_3O_4) by means of simple, aqueous chemistry is presented starting from TcO_4^- in 5 M nitric acid. A combination of X-ray diffraction and X-ray absorption fine structure spectroscopy reveals that Tc(IV) replaces Fe(III) within the iron oxide structures. Following incorporation, Tc doped samples were suspended in deionized water under aerobic conditions, and the release rates of Tc under these conditions were determined. The results of this work show that Tc leaches more quickly from Fe_3O_4 than from α-Fe_2O_3 or $MgFe_2O_4$. Modeling the leach rates and comparison with the leach rate of Tc from TiO_2 indicate that release of Tc is controlled by solid state diffusion.

Introduction

Technetium (^{99}Tc) is a long lived (2.1×10^5 yr), high yield (6 %) fission product that presents unique challenges to nuclear waste disposal due to the environmental mobility of pertechnetate (TcO_4^-) under aerobic conditions.[1-4] The most effective method for preventing Tc migration is disposal in an anaerobic repository since the stable form of Tc under anaerobic conditions, Tc(IV), is not highly mobile.[3] Another potential method for preventing Tc migration from a waste repository is stabilizing it within a durable waste form that can sequester ^{99}Tc until it has decayed. A general rule of thumb is that ten half-lives is sufficient time to allow a radionuclide to decay; however, this period can be shorter or longer depending on the risks posed by the radionuclide.[5] In the U.S., all of the operational and proposed repositories for spent nuclear fuel (Yucca Mountain) and for fission products generated during plutonium production (Savannah River Site and Hanford Reservation) are aerobic and/or near-surface sites.[6-8] The disposal of ^{99}Tc in these aerobic repositories drives the interest in waste forms for ^{99}Tc that are stable in aerobic environments.

Even under anaerobic conditions, the solubility of Tc(IV), 3 pM, is still greater than the U.S. Environmental Protection Agency maximum contaminant level for drinking water of 900 pCi/L or 0.5 pM.[9-11] In addition, the solubility of Tc(IV) can be increased by ubiquitous natural ligands such as humic substances.[12-14] Consequently, durable waste forms for ^{99}Tc would improve the performance of anaerobic waste forms. Borosilicate glass, the most widely used nuclear waste form, is likely to durably sequester ^{99}Tc; however, Tc species can evaporate from molten glass at vitrification temperatures, 1100 °C to 1200 °C, which complicates the incorporation of ^{99}Tc.[15-21] The best studied alternative to glass is the synthetic titanate mineral Synroc, which is highly durable.[22] Certain iron oxide minerals are also highly durable under aerobic conditions.[23] Both hematite (α-Fe_2O_3) and goethite (α-FeOOH) are well known to be stable under aerobic conditions.[24-28] In addition, yttrium iron garnet (YIG) has been suggested as a single-phase nuclear waste form due to its ability to accommodate ions with varying charges and radii.[29, 30] The similarity of the ionic radius of six-coordinate Tc(IV), 0.645 Å, to that of Fe(III), 0.645 Å,[31] respectively, suggests that Tc(IV) can replace Fe(III) in an iron oxide provided that the difference in charge is balanced.[23] Under reducing conditions, trivalent iron oxides like α-Fe_2O_3 are unstable towards reduction; however, ^{99}Tc migration is significantly slower under such conditions.[3] Unlike goethite and

hematite, magnetite (Fe_3O_4) is not stable under aerobic conditions. Upon exposure to air, magnetite is oxidized to maghemite (γ-Fe_2O_3), which is unstable with respect to hematite and goethite.

Previous studies have demonstrated that Tc(IV) can be incorporated into other iron oxides, and the subject has been recently reviewed.[32] Treatment of green rust with pertechnetate resulted in Tc(IV) incorporation into an iron oxide phase.[33] Long tem exposure of magnetite to pertechnetate solutions resulted in reduction of TcO_4^- to Tc(IV), and incorporation of Tc(IV) into the crystal lattice of Fe_3O_4.[34, 35] Initial adsorption of Tc(IV) onto ferrihydrite resulted in incorporation of Tc(IV) in the resulting magnetite phase.[36] Smith, et al. studied Tc-doped magnetite computationally and found that Tc(IV) doping into the octahedral Fe sites is possible, but other Tc oxidation states, especially Tc(V), may be present and several mechanisms can balance the charge mismatch created when Tc(IV) replaces Fe(III) on the octahedral site.[37] More recent computational studies of Tc doping into Fe_3O_4 and $MgFe_2O_4$ indicate that the charge may be balanced by either replacement of Fe(III) by Fe(II) or by creating octahedral vacancies.[37] Incorporation of Tc into hematite has also been studied computationally, and up to 2.6 wt. % of isolated Tc(IV) can be accommodated by hematite when the charge is balanced by reduction of a neighboring Fe(III) site to Fe(II).[28] Furthermore, treatment of alkaline solutions containing TcO_4^- and CrO_4^{2-} with white rust, $Fe(OH)_2$, results in incorporation of both transition metals into the magnetite structure.[38] To address the aforementioned problem of Tc(VII) volatility during glass vitrification, transition metal doped magnetite has been studied and Ni and Co-doped magnetite were found to reduce the extent of Tc(IV) oxidation to volatile Tc(VII) during high temperature treatment.[19] Finally, Tc-doped goethite has been investigated both experimentally and computationally.[39-41]

While less abundant than hematite and goethite, high nickel magnesioferrite, $Ni_xMg_{1-x}Fe_2O_4$ is also highly durable as shown by its persistence since being created 65 million years ago by the Chixulub meteorite impact.[42-45] In contrast to Fe_3O_4, which is an inverse spinel where the tetrahedral sites are occupied by Fe(III), in $MgFe_2O_4$ both Mg(II) and Fe(III) can be present in both the octahedral and tetrahedral sites.[46] Spinel ferrites, such as magnesioferrite, can be prepared quickly in water, which make them attractive from a process perspective.[47-53] While incorporation of Tc(IV) into spinel ferrites has been studied previously, the previous synthetic route, addition of TcO_4^- to dissolved ferrous sulfate followed by treatment with sodium hydroxide and sodium nitrate, would create significant amounts of secondary waste if used in conjunction with spent nuclear fuel reprocessing.[54] In addition, $MgFe_2O_4$ could not be prepared in the previous study due to the precipitation of magnesium sulfate.

The primary aims of this study were to develop simple routes to Tc doped iron oxides starting from TcO_4^- in nitric acid and to determine the rate of leaching of Tc from the resulting materials. The starting point, TcO_4^- in 5 M nitric acid, is a surrogate for the Tc waste stream from the UREX+ family of separations.[55] While UREX+ waste streams contain higher concentrations of nitric acid, the concentration may be reduced to ~5 M by air stripping.[56] The chemistry described here is also applicable to the PUREX waste stream, which has a lower nitric acid concentration, 1.6 M.[57] The TcO_4^- in nitric acid was first denitrated by reaction with formic acid.[56] This denitrated solution was treated with iron powder to produce ferrous nitrate *in situ.*[58] The ferrous nitrate is both the iron oxide precursor and the reductant used to reduce TcO_4^- to Tc(IV). Modifications of the experimental procedure resulted in specific iron oxides doped with Tc. The resulting materials were characterized by X-ray diffraction (XRD) and extended X-ray absorption fine structure (EXAFS) spectroscopy, which indicate that Tc(IV) replaces Fe(III) in the lattice. The release of Tc from the Tc-doped iron oxides into aerated, deionized water was followed for 200 days, to examine the hypothesis that magnesioferrite would be more effective than magnetite at retaining Tc.

Experimental

Caution. ^{99}Tc is β-emitter. All operations were carried out in a laboratory equipped to handle this isotope. All handling of uncontained Tc and all reactions were carried out in a fume hood that was posted as a radioactive contamination area.

General. Iron powder, 99.5% purity, <10 um size, was obtained from Alfa Aesar. Deionized (DI) water was obtained from a Milli-Q Gradient A-10 system. Solid NH_4TcO_4 was obtained from Oak Ridge National Laboratory, and dissolved in 0.03 M HNO_3. Other chemicals were ACS grade or better and were used as received. pH was determined using an Orion ROSS pH electrode and a VWR pH meter. The pH meter was calibrated daily using pH 4 and pH 7 buffers or pH 10 and pH 7 buffers.

Denitration of TcO_4^- in 5 M HNO_3.[59] (This procedure is from ref. 59, and is repeated here for clarity). A 25 mL, three-neck, round bottom flask was equipped with a stirbar, glass stopper, heating mantle, and a reflux condenser capped with a tee connecting it to a bubbler and an argon line. The flask was purged for 5 minutes with argon. 8.00 mL of 5.18 M HNO_3 was added to the flask, followed by 70 uL of 0.15 M TcO_4^- in 0.03 M HNO_3 (1.0 mg of ^{99}Tc). The flask was equipped with a PTFE-faced silicone septum, and the solution was degassed with a stainless steel needle. The solution was heated to reflux, and sparging was stopped. HCOOH (2.35 mL) was added to the hot HNO_3 solution via a syringe pump (KD Scientific) at a rate of 1.5 mL hr^{-1}.[56, 60] After heating the pale yellow solution at reflux for 4 hours, a colorless, denitrated solution was obtained. The pH of this solution varied from 0.5 to 1. Titration of a control experiment without Tc showed that this solution contained 0.5 M H^+. Since the solution had pH = 1, the denitrated solution contained 0.1 M HNO_3 and 0.4 M HCOOH.

Tc-doped Fe_3O_4 (1). The denitrated solution was cooled to room temperature and iron powder (28 mg, 0.50 mmol) was added while purging with Ar. After stirring for 5 min, the Fe powder had dissolved forming a dark red-brown solution. 14.8 M NH_4OH (0.5 mL, 7.4 mmol) was added by syringe, and the mixture immediately turned black. The mixture was heated at reflux for one hour then allowed to cool. The mixture was divided among five 2 mL polypropylene (PP) centrifuge tubes. The colorless supernate (8.3 mL, pH 8.7), was separated by centrifugation. LSC of 10 uL of the supernate (17.7 Bq, 1050 dpm) showed that 2.3 % of Tc was in solution. The black solid was combined in a single centrifuge tube. It was washed twice with 1.5 mL water then by 1.5 mL acetone. Based on the mass of Fe, the composition of sample **1** is $Tc_{0.06}Fe_{2.94}O_4$ (2.5 wt. % Tc).

EXAFS sample (1'). As described for **1** except that 100 uL of TcO_4^- stock (1.4 mg Tc) was used in the denitration experiment rather than 70 uL (1.0 mg Tc).

Tc-doped $MgFe_2O_4$ (2) The denitrated solution was cooled to room temperature and iron powder (28 mg, 0.50 mmol) was added while purging with Ar. The initially pink solution was purged with Ar while heating it to reflux. After 5 min, the Fe powder had dissolved forming a dark red-brown solution. $Mg(OH)_2$ (30 mg, 0.51 mmol) was added under a vigorous Ar purge. The $Mg(OH)_2$ dissolved leaving the appearance of the solution unchanged. 14.8 M NH_4OH (0.5 mL, 7.4 mmol) was then added by syringe, and the mixture immediately turned black and viscous. The mixture was heated at reflux for 1 hour and allowed to cool. The mixture was divided among five 2 mL polypropylene (PP) centrifuge tubes. The colorless supernate (6.6 mL, pH 7.8), was separated by centrifugation. LSC of 10 uL of the supernate (61.2 Bq, 3730 dpm) showed that 7.9 % of Tc was in solution. The dark brown solid was combined in a single centrifuge tube. It was washed twice with 1.5 mL water then by 1.5 mL acetone. Based on the mass of Fe, the composition of sample **2** is $Tc_{0.03}Mg_{1.03}Fe_{1.94}O_4$ (2.0 wt. % Tc).

Tc-doped α-Fe_2O_3 (3). The denitrated solution was cooled to room temperature and iron powder (28 mg, 0.50 mmol) was added while purging with Ar. The initially pink solution was purged with Ar while heating it to reflux. After 5 min, the Fe powder had dissolved forming a yellow-green solution. 14.8 M NH_4OH (0.5 mL, 7.4 mmol) was added by syringe, and the mixture immediately turned black and viscous. The mixture was heated at reflux for 18 hours. The resulting brick red mixture was allowed to cool. The mixture was divided among five 2 mL polypropylene (PP) centrifuge tubes. The colorless supernate (8.7 mL, pH 3.3), was separated by centrifugation. LSC of 10 uL of the supernate (127 Bq, 7640 dpm) showed that 18 % of Tc was in solution. The brick red solid was combined in a single centrifuge tube. It was washed twice with 1.5 mL water then by 1.5 mL acetone. Based on the mass of Fe, the composition of sample **3** is $Tc_{0.03}Fe_{1.97}O_3$ (2.2 wt. % Tc).

Leaching experiment. All handling was performed in air using solutions equilibrated with air. Tc doped iron oxide samples were suspended in 10.0 mL DI water and transferred to 15 mL PP centrifuge tubes. The samples were then dispersed by sonication. To keep the iron oxide in suspension, the centrifuge tubes were placed on a rocking table at 0.5 Hz. The Tc concentration was measured by LSC as described below. Material removed for

LSC analysis was re-suspended by sonication and placed back into the original centrifuge 15 mL tubes. The total amount of Tc was determined from the amount of Tc in the solid minus the Tc used to prepare the XRD samples, which was 6 % as determined by direct counting. The amount of Tc released into solution was calculated from the Tc concentration by LSC using the initial volume of water, 10.0 mL. The tubes holding the Tc in **2** and **3** leaked slightly (~1.5 mL lost) after 100 days as determined by the detection of Tc contamination on the rocking table. Loss of liquid water from samples **2** and **3** will have little effect on the results since loss of solution does not change the Tc concentration. However, loss of water vapor will lead to a higher concentration of Tc in solution, and the fraction of Tc leached from the solid will be artificially high.

At the end of the experiment, the solids were isolated by distributing each sample among 6 PP centrifuge tubes and centrifuging them (5 min, 8500 g). The solids were collected and washed once with 1.5 mL water followed by 1.5 mL acetone. The materials isolated after leaching samples **1**, **2**, and **3** are **1a**, **2a**, and **3a**, respectively.

Liquid Scintillation Counting (LSC). 1.8 mL of the solution containing suspended iron oxide particles were added to a 2 mL PP centrifuge tube. The sample was centrifuged for 5 min at 8500 g. 1 mL of the supernate in this tube was carefully removed and added to a clean 2 mL PP centrifuge tube. This new sample was centrifuged for 5 min at 8500 g. 10 uL of this doubly-centrifuged solution was then added to a scintillation vial containing 4 mL Ecolume. Samples were counted using a Wallac 1414. Results were not corrected for chemical quench. Comparison of the spectral quench parameter, SQP(E), to a ^{99}Tc quench curve prepared using nitromethane showed <1% quenching.

X-ray diffraction (XRD). Tc-doped iron oxide was suspended in acetone by sonication. A drop of the suspension was placed a silicon zero background plate and allowed to dry (60 s). A Kapton film was carefully placed over the sample and sealed to the sample holder to prevent the spread of contamination. Diffraction data was obtained with a Panalytical X'Pert Pro diffractometer using either a Co or Cu source (all data is presented as 2θ plots for Co K X-rays). For both the Cu and Co sources, the diffractometer precision and line shape parameters were determined using a NIST Si standard (640d). Data were obtained as several 2 hour scans which were averaged using HiScore Plus.[61] The diffraction data were modeled using the crystal structures of magnetite, magnesioferrite, or hematite. X'Pert High Score Plus software was used to perform Rietveld refinements of the data to determine the lattice parameters and sizes of the crystallites.

EXAFS measurements. Sample **1'** was dispersed in water, centrifuged (5 min, 8500 g), and the liquid was discarded to produce a homogeneous pellet. Samples **2a** and **3a** were thoroughly mixed with boron nitride. The mixtures were contained in aluminum holder sealed with Kapton tape. All spectra were obtained at the Tc K edge (21 keV). Spectra were recorded at ambient temperature using Beamline 11-2 at the Stanford Synchrotron Radiation Lightsource. A double-crystal monochromator with Si [220] $\phi = 90$ crystals was used to select the energy, and the second crystal was detuned by 50% to decrease the harmonic content of the beam. For sample **1'**, a transmission spectrum was recorded using argon filled ion chambers. For samples **2a** and **2b,** fluorescence spectra were obtained using a 100 channel high-purity Ge detector and were corrected for detector deadtime.

EXAFS data were analyzed using the "shell-by-shell" approach[62] with ifeffit[63] and Artemis/Athena.[64] Theoretical scattering curves for the various iron oxides were calculated with Feff6.[65] For these calculations, Tc replaced an Fe(III) ion. For Fe_3O_4 and $MgFe_2O_4$ Tc replaces Fe(III) in the octahedral site; α-Fe_2O_3 has only a single Fe site.[66] The EXAFS model included both Tc(VII) in TcO_4^- and Tc(IV) replacing Fe in an iron oxide. For each Tc oxidation state, the coordination numbers are determined by the value in that specific compound (e.g. 6 O nearest neighbors for Tc in iron oxide and 4 O for TcO_4^-). The fraction of Tc in the phases was allowed to vary during refinement, but the sum of fractions was constrained to unity (e.g. 0.15 Tc in TcO_4^- and 0.85 Tc in Fe_3O_4). The coordination number of the scattering atoms in the fit was determined by the fraction of the oxidation state present multiplied by the number of neighbors for that shell in that oxidation state (e.g., for the 0.85 Tc in Fe_3O_4, there are 5.1 oxygen nearest neighbors at 2 Å). Scattering shells were removed from the fit if they did not decrease the value of reduced χ^2. Once the fit was complete, an F-test was performed on each shell to determine the significance of its contribution to the total fit.[67] The p-factor from the F-test indicates the likelihood that the improvement to the fit due to a given shell is due to random error.

Results

Incorporation of Tc into iron oxides. The primary goal of this work was to develop methods of incorporating Tc(IV) into iron oxides starting from TcO_4^- in 5 M nitric acid. Following chemical denitration using formic acid, $Fe(NO_3)_2$ (aq) was formed *in situ* by dissolving Fe powder in the denitrated solution.[58] When this solution was neutralized with NH_4OH, a black slurry formed. After heating for one hour at reflux, Tc-doped Fe_3O_4 (**1**) was isolated, and LSC analysis of the supernate showed that 97 % of the TcO_4^- was removed from solution. Tc-doped $MgFe_2O_4$ (**2**) was prepared identically to **1** except that $Mg(OH)_2$ was added prior to neutralization with NH_4OH. Preparation of **2** removed 92 % of the TcO_4^- from solution. Tc-doped α-Fe_2O_3 (**3**) was prepared identically to **1** except that the mixture was heated at reflux for 16 hours rather than 1 hour. During reflux, ammonia was lost from solution, and the pH decreased to 3.3. At low pH, hematite rather than goethite is the stable Fe(III) oxide.[68-70] Synthesis of **3** removed 82 % of Tc from solution. A duplicate synthesis of **3** ended with a slightly higher pH, 3.4, and contained goethite in addition to hematite. As shown by Babčan at 100 °C in the iron sulfate system, both hematite and goethite can be formed at these pHs while only goethite is formed at higher pH.[70] The presence of only hematite in **3** rather than a mixture of hematite and goethite may have been fortuitous or it may have been due to the lower pH.

Leaching of ^{99}Tc from Tc-doped iron oxides. Leaching experiments were performed by suspending the iron oxide samples in deionized water in air at room temperature (ca. 20 °C). Samples were removed from the tubes to determine the amount of Tc in solution by LSC (Figure 1). All samples quickly lost approximately 5 % of the Tc, and **1** continued to leach Tc relatively quickly. For **2** and **3**, the leaching of Tc slowed greatly after day 5. The final pH of the solutions were 7.2, 7.2, and 4.1 for **1-3**, respectively. Samples **2** and **3** leaked slightly (~1.5 mL of lost volume) during the second half of the leaching experiment. If only liquid water leaked, the results should be largely unaffected as loss of the solution does not change the concentration of Tc. However, if significant amounts of water vapor were lost in addition to liquid water, the Tc concentration in solution will increase, and the amount of Tc leached from samples **2** and **3** will be slightly smaller than shown in Figure 1 for the last two data points.

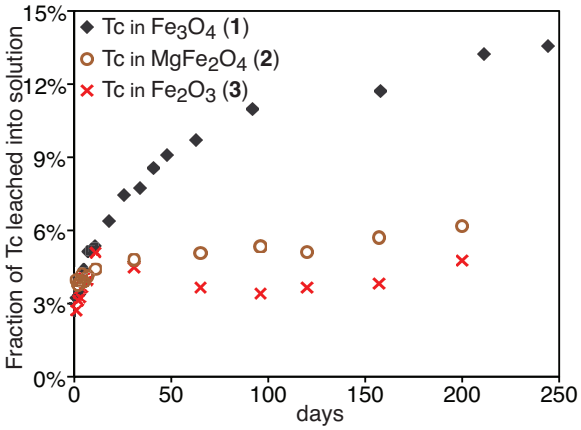

Figure 1. Fraction of ^{99}Tc leached from Tc-doped iron oxides into aerated DI water

The rise and fall in the amount of Tc in solution for sample **3** from day 1 through 60 is believed to be due to the presence of hematite nanoparticles that could not be easily removed from solution by centrifugation. As the samples aged, the nanoparticles presumably agglomerated and were more effectively removed by centrifugation; however, early sample readings are likely artificially high due to the presence of Tc in inseparable hematite nanoparticles. Similar behavior was seen previously in Tc-doped TiO_2 nanoparticles.[59] In contrast, Tc-doped Fe_3O_4 nanoparticles, both in this study and a previous one,[54] rapidly agglomerate and precipitate.

X-ray diffraction. The XRD patterns were recorded before and after leaching and are shown in Figure 2. The results of Rietveld refinement are given in Table 1. In each sample, a single oxide phase is present. The lattice parameters provide information about the manner in which the charge mismatch created by replacing Fe(III) by Tc(IV) is balanced. If the charge is balanced by replacing a neighboring Fe(III) by Fe(II) or Mg(II), the lattice

parameter of the Tc-doped oxide will be larger than in the parent compound.[54] If the charge is balanced by creating octahedral site vacancies (analogous to maghematization), the lattice parameter will be smaller than in the parent compound. In **1**, the lattice parameter is somewhat smaller than in Fe_3O_4,[71] indicating that the magnetite host is somewhat oxidized (maghematized),[72] and the effect of charge balance by formation of vacancies is greater than by replacing Fe(III) by Fe(II). On the other hand, the lattice parameter of **3** is larger than α-Fe_2O_3, which suggests that the charge is largely balanced by replacing Fe(III) with Fe(II). Finally, the lattice parameter of **2** is identical to $MgFe_2O_4$,[46] which suggests that the charge mismatch created by replacing Fe(III) with Tc(IV) is balanced by a combination of vacancies and Mg(II) and/or Fe(II) replacing Fe(III).

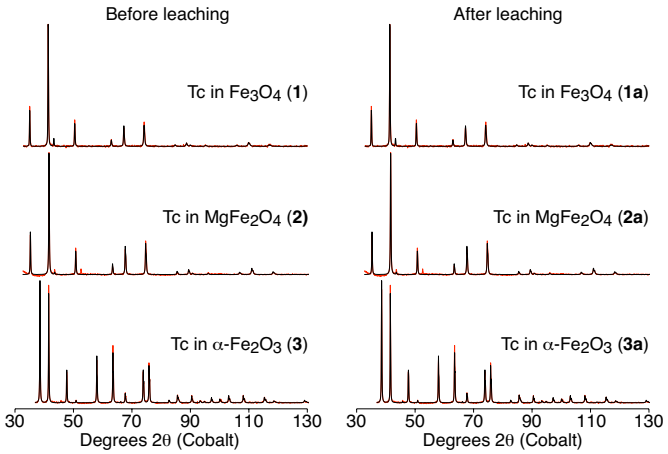

Figure 2: X-ray powder patterns (in red) and Rietveld fits (black) of **1-3**. Data are normalized such that the largest peaks have the same height, and patterns are shown with the background removed.

Table 1: Diffraction results for samples 1-3 before and after leaching

Sample	Phase	a (Å)	c (Å)	Crystallite size (nm)	pH
1	Fe_3O_4	8.3948(2)		74	
1a-after	Fe_3O_4	8.3873(3)		56	7.2
2	$MgFe_2O_4$	8.3850(3)		73	
2a-after	$MgFe_2O_4$	8.3752(2)		67	7.2
3	α-Fe_2O_3	5.0347(1)	13.7896(3)	99	
3a-after	α-Fe_2O_3	5.0351(1)	13.7943(2)	118	4.1

Lattice parameters of the parent compounds: Fe_3O_4 (8.3958 Å), $MgFe_2O_4$ (8.3805 Å),[46] γ-Fe_2O_3 (8.3419 Å), [72, 73] α-Fe_2O_3 (a = 5.0335 Å, c = 13.7471 Å).[74]

As illustrated in Figure 2, no new phases were observed after leaching, which indicates that these samples are stable towards transformation to other mineral phases over the duration of the experiment. However, both the lattice parameters and the apparent sizes of the crystallites change upon leaching. In samples **1a** and **2a**, the lattice parameters decrease, which indicates partial maghemitization of these samples (some Fe(II) or Mg(II) is lost to solution and additional vacancies are created). Samples **1a** and **2a** are not fully converted to maghemite (γ-Fe_2O_3), however. Their lattice parameters are much closer to those of Fe_3O_4 and $MgFe_2O_3$ than they are to that of γ-Fe_2O_3.[72] The lattice parameters of **3** also change after leaching although they change less and change in the opposite direction (c is slightly larger after leaching). The size of the crystallites in **3**, estimated from the peak profile parameters, increases slightly upon leaching as expected due to Ostwald ripening. On the other hand, the sizes of the crystallites in **1a** and **2a** appear to decrease upon leaching, which is unlikely. Although the nanoparticles will initially dissolve until the concentration of Fe(III) reaches equilibrium, the amount of Fe(III) in solution is so low (< 10^{-7} M at pH 7) that only a tiny fraction of the samples dissolve.[75] Another source of diffraction peak broadening is a distribution of lattice parameters. This effect has previously been observed in

magnetite nanoparticles and is attributed to particle size effects. Smaller particles have a higher surface to volume ratio and consequently oxidize at a greater rate. Since the lattice parameter is inversely proportional to the degree of oxidation, more oxidized particles have smaller lattice parameters. As a result, a distribution of magnetite particle sizes results in a distribution of lattice parameters and broadening of the diffraction peaks. In **1a** and **2a**, we cannot determine the relative contributions of particle size and lattice parameter variation from the diffraction pattern, and both contributions will be reflected in the estimated particle size. In other words, the apparent decrease in crystallite size observed for **1a** and **2a** is likely due to a distribution of lattice parameter values rather than shrinking crystallites.

EXAFS spectroscopy of Tc doped iron oxides. While the diffraction data indicates the identities of the iron oxide phases present in the samples, they do not provide direct evidence that Tc is incorporated into the lattice (e.g., Tc(IV) replaces Fe(III) versus being present as a separate phase such as $TcO_2 \cdot xH_2O$ or a surface precipitate). To determine whether Tc is incorporated into the lattice, the Tc K-edge EXAFS spectra of the samples were studied. The spectra and fits are shown in Figure 3 and the fitting parameters are given in Table 2. The data for **1'** was obtained on a sample that had not been leached, while the data for **2a** and **3a** are from samples isolated after leaching. In all cases, Tc is largely present as Tc(IV) as indicated by the 2.0 Å distance to neighboring oxygen atoms. In addition, a small amount of TcO_4^- may be present in the samples as indicated by the presence of O neighbors at 1.7 Å. In all cases, the data are consistent with Tc(IV) replacing Fe(III) on octahedral sites as previously observed.[34, 36, 54]

The EXAFS data and fit for sample **1'** are very similar to those previously reported for Tc-doped Fe_3O_4.[54] The EXAFS fits are consistent with Tc(IV) occupying the octahedral sites of Fe_3O_4. As previously observed, Tc is not homogeneously distributed in Fe_3O_4. It is present in regions of high Tc concentration. The Tc local environment is most similar to that of Ti in ulvöspinel ($TiFe_2O_4$) in that the Tc has 2-3 Tc neighbors, and the Tc-Fe distances are closer to the Ti-Fe distances in $TiFe_2O_4$ than to the Fe-Fe distances in Fe_3O_4. In **1'**, most of the neighboring Fe (both octahedral and tetrahedral sites) must be present as Fe(II) to balance the charge.

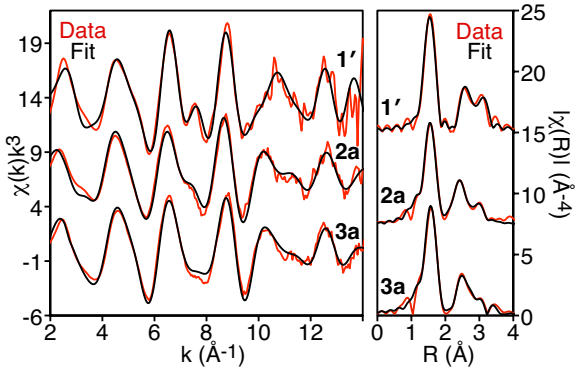

Figure 3. Tc K-edge EXAFS spectra of Tc in iron oxides (left) and Fourier transforms (right). Data are shown in red and EXAFS fits are shown in black for Tc in Fe_3O_4 (**1'**), Tc in $MgFe_2O_4$ (**2a**), Tc in Fe_2O_3 (**3a**).

Table 2. Local environment of Tc in iron oxides from Tc K-edge EXAFS fitting

Neighbor	#	R (Å)	σ^2 (Å^2)	p	Fe local structure
Tc doped Fe_3O_4 (**1'**)[a]					
O	0.5(1)	1.68(1)	0.001	0.002	--
O	5.3(2)	2.025(6)	0.0046(5)	<0.001	6O@2.06 Å
Fe	2.7(2)	3.13(2)	0.0014(8)	<0.001	
Tc	2.6(3)	3.13(2)[b]	0.0014(8)[b]	0.002	6Fe@ 2.98 Å
Fe	5.3(2)	3.46(1)	0.008(3)	0.378	
O	7.0(2)	3.57(5)	0.008(3)[b]	0.078	6Fe@3.4 Å
(MS)[c]	5.3(2)	4.05(1)	0.008(3)[b]	0.018	
Tc doped $MgFe_2O_4$ after leaching (**2a**)[d]					
O	0.35(8)	1.73(2)	0.001[b]	0.003	--
O	5.5(1)[c]	2.046(8)	0.0065(5)	0.001	6O@2.0 6Å
Fe	1.0(9)[d]	3.00(5)	0.007(1)	0.260	
Mg	3.2(7)[d]	3.00(5)	0.007(1)[e]	0.009	6Fe/Mg@2.96 Å
Tc	1.2(1.2)[c]	2.602(9)	0.007(1)[e]	<0.001	
Fe	2.0(1.0)[c]	3.45(5)	0.010(3)	0.286	6Fe/Mg@3.47 Å
Mg	3.5(1.0)[c]	3.45(5)	0.010(3)[e]	0.132	
(MS)[c]	5.5(1)[c]	4.09(2)[f]	0.017(1)	0.124	
Tc doped α-Fe_2O_3 after leaching (**3a**)[e]					
O	0.3(1)	1.73(2)	0.001[b]	0.010	--
O	5.6(1)[c]	2.041(7)	0.0062(5)	<0.001	6O@1.87-2.09 Å
Tc	0.8(7)[d]	2.61(1)	0.008(1)	0.003	1Fe@2.94 Å
Fe	3.2(7)[d]	3.05(1)	0.008(1)	0.008	3Fe@2.99 Å
Fe	2.8(1)[c]	3.49(2)	0.009(2)	0.091	3Fe@3.42 Å
O	5.6(1)[c]	3.19(3)	0.009(2)[e]	0.018	6O@3.5-3.7Å
Fe	5.6(1)[c]	3.70(3)	0.016(4)	0.094	6Fe@3.7-3.8 Å

[a] Fit range 2<k<13, 1<R<4.2, DE_0 = 2(1) eV, 22.7 independent data. 11 parameters, R=0.019. [b] Parameter constrained to equal that of the preceding shell. [c] Tc-O-Tc-O multiple scattering path. [d]Fit range 2<k<14; 1<R<4, DE_0 = -2(1) eV, 24.6 independent data, 14 parameters, R=0.017. [e]Fit range 2<k<14; 1<R<4, DE_0 = 3(1) eV, 24.6 independent data, 14 parameters: R=0.021.

For **2a**, the EXAFS data and fit are similar to that of **1'** with some differences. As indicated in Table 2, the metal ions in the vicinity of Tc are better modeled by Mg than by Fe, which is consistent with substitution of Fe(II) in **1** by Mg(II) in **2** as hypothesized. In addition, the data for **2a** were better modeled with a shorter Tc-Tc distance than in **1'**. This short distance is consistent with the presence of a Tc-Tc bond between Tc(IV) atoms on adjacent octahedral sites, as previously seen in Tc-doped TiO_2 as well as a variety of dinuclear Tc(IV) complexes.[59, 76-79] Overall, the EXAFS data and fit are consistent with pairs of Tc(IV) ions replacing pairs of Fe(III) on adjacent octahedral sites in $MgFe_2O_4$.

For **3a**, the EXAFS data are consistent with Tc(IV) replacing Fe(III) in the hematite lattice. The local structure of Fe(III) in hematite is considerably different from that in inverse spinels. In hematite, Fe(III) has a trigonally distorted octahedral oxygen environment. The structural unit is a pair of face-sharing Fe(III) ions with a 2.94 Å Fe-Fe distance. Each Fe has three more Fe neighbors at 3 Å and a further three Fe neighbors at 3.4 Å. As shown in Table 3, the best fit for **3a** is obtained with a pair of face-sharing Tc(IV) ions replacing a pair of Fe(III) ions. The short 2.6 Å Tc-Tc distance, presumably due to presence of a Tc-Tc bond, is similar to that of other species with a Tc-Tc bond.[59, 76-79] To balance the charge, some of the neighboring Fe(III) ions must be replaced by Fe(II). Correspondingly, the distances to neighboring Fe atoms will be somewhat longer than in α-Fe_2O_3 as indicated in Table 3. The structure of Tc in hematite has previously been investigated computationally using a single Tc(IV)/Fe(II) pair in a hematite super cell.[28] In that case, Tc(IV) behaves similarly to Ti(IV) in ilmenite ($FeTiO_3$) where a face-sharing Ti(IV)/Fe(II) pair replaces the pair of face-sharing Fe(III) ions in hematite. Nevertheless, the computational results indicated that at least 2.6 wt. % Tc would be stable in hematite, which is greater than the 2.2 wt. % of Tc incorporated into hematite in this study.

In all cases, the EXAFS results indicate that Tc(IV) enters the lattice of the iron oxides by substitution for Fe(III). However, the EXAFS data alone are not sufficient to identify the iron oxide phase. Unambiguously assigning the iron phase occupied by Tc depends upon the distances and coordination numbers for the next-nearest set of metal neighbors (in Fe_3O_4, these are the tetrahedral Fe neighbors at 3.45 Å). This is challenging because the distances and coordination numbers of this shell of iron neighbors are very similar for most iron oxides. While these neighboring atoms refine to the correct distances in the EXAFS fit, the improvement to the fit from including these scattering atoms is not significant enough to unambiguously indicate that these atoms are present as indicated by their p-factors, which are greater than 0.05. However, the combination of XRD and EXAFS results, along with the fact that the EXAFS data are well modeled by the Fe-Fe distances in the iron oxide phases determined by XRD, strongly indicate that Tc(IV) replaces Fe(III) in the iron oxide phases identified by XRD.

Discussion

As shown above, Tc doped iron oxides may be prepared from TcO_4^- doped nitric acid using iron powder and NH_4OH or a combination of $Mg(OH)_2$ and NH_4OH. The approach is simple, and the formation of the spinel phases, magnetite and magnesioferrite, requires only one hour at reflux. Formation of the Tc-doped hematite is much slower and presumably involves the dissolution and recrystallization of the initially formed Tc-doped magnetite. This project is somewhat analogous to the work of Um and coworkers who have used $Fe(OH)_2$ to remove TcO_4^- from alkaline solutions, especially simulants of low activity waste streams at the Hanford Site, and incorporate it into a variety of iron oxides including goethite, magnetite, cobalt ferrite, and nickel ferrite.[37-40] The primary goal in that work is stabilizing Tc during vitrification to decrease its volatility. The primary goal of the work presented here is removing Tc from acid waste streams during reprocessing of spent nuclear fuel and stabilizing the Tc in a form that may be easily handled and ultimately converted to a durable nuclear waste form.

From the standpoint of the long-term disposal of nuclear waste, the most important factor is understanding how well the materials retain Tc. The leaching data can be used to address two issues related to the retention of Tc. First, how effective are these specific samples (iron oxide nanoparticles) at retaining Tc? Second, how effective are iron oxides matrices for immobilizing Tc? The latter are indicated by the normalized release rates (LR) of the samples. For **1**-**3**, LR(Tc) may be calculated using eq 1 where ρ is the density of the iron oxide, m is the mass of the sample, f_{Tc} is the fraction of Tc in the solid, m_{Tc} is the mass of Tc lost, D is the crystallite diameter from XRD, and t is the time in days.[80]

$$LR(Tc) = \frac{m_{Tc} \cdot \rho \cdot D}{6m \cdot f_{Tc} \cdot t} \qquad (1)$$

In **2** and **3,** the apparent amount of Tc in solution initially decreases, which is likely due to the presence of Tc-doped FeO_x nanoparticles as mentioned above. The normalized release rates for **1**-**3** are 4×10^{-5} g m^{-2} d^{-1}, 2×10^{-5} g m^{-2} d^{-1} and 2×10^{-5} g m^{-2} d^{-1}, respectively, at the end of the leaching period (244 d for **1** and 200 d for **2** and **3**). The release of Tc from $MgFe_2O_4$ and Fe_2O_3 is slower than from Fe_3O_4 as hypothesized based on the lower environmental durability of Fe_3O_4 relative to the durability of $MgFe_2O_4$ or Fe_2O_3.

The normalized release rates of Tc from **1-3** may be compared to those of boron from high-level borosilicate waste glass (B and Tc have similar leach rates) and Ti from the durable titanate ceramic Synroc (Tc replaces Ti and their normalized release rates should be similar).[81-85] Borosilicate high-level waste glass has a LR for boron of 1×10^{-3} g m^{-2} d^{-1} at 23 °C for 62 days.[86, 87] In Synroc C, the measured LR for Ti is is 2×10^{-5} g m^{-2} d^{-1} at 95 °C;[22] the calculated LR for Ti at 21 °C is 2×10^{-6} g m^{-2} d^{-1} using the activation energy for leaching from Synroc, 30 kJ mol^{-1}.[80] Over a similar period of time, Tc is leached from **1-3** at 1×10^{-4} g m^{-2} d^{-1}, 4×10^{-5} g m^{-2} d^{-1} and 5×10^{-5} g m^{-2} d^{-1}, respectively. While the normalized Tc release rates from iron oxides are lower than from borosilicate waste glass, they are greater than those of titanium based ceramics, either Synroc, LR(Ti) is 2×10^{-6} g m^{-2} d^{-1}, or Tc-doped TiO_2, where the lowest LR(Tc) is 3×10^{-6} g m^{-2} d^{-1}.[59] These results indicate that iron oxides could be more effective matrices for retaining Tc than borosilicate glass; however, iron oxides are less effective than titanates. However, these results do not indicate that **1-3**, which are nanoparticles, should be considered as effective waste forms for Tc without further manipulation.

To evaluate how well these samples would retain ^{99}Tc, two empirical models were used - loss of Tc due to dissolution of particles (dissolving particle) and slow diffusion of Tc(IV) from particles (diffusion model).[88] The time needed for all of the Tc to enter the solution, τ, is given by eqs 2 and 3 for the dissolving particle and diffusion models, respectively, where m_{fast} is a variable corresponding to the rapid loss of Tc at the beginning of the experiment.[88] Results are shown in Figure 4. Using the dissolving particle model, Tc would be leached from **1-3** after 8.5 yr, 41 yr, and 30 yr, respectively. If the diffusion model is applicable, Tc would be leached from **1** to **3**, after 240 yr, 2800 yr, and 740 yr, respectively. Substitution of Fe(II) by Mg(II) in **2** greatly reduces the rate of Tc loss to solution relative to **1** as originally hypothesized based on the greater durability of $MgFe_2O_4$ in the environment. While both the dissolving particle and diffusion models fit the leaching data for **2** and **3** equally well, release of Tc from **1** is consistent only with the diffusion model.

$$\frac{t}{\tau}=1-\left(1-m_{Tc}-m_{fast}\right)^{2/3} \qquad (2)\ \text{dissolving particle}$$

$$\frac{t}{\tau}=1-3\left(1-m_{Tc}-m_{fast}\right)^{2/3}+2\left(1-m_{Tc}-m_{fast}\right) \qquad (3)\ \text{diffusion}$$

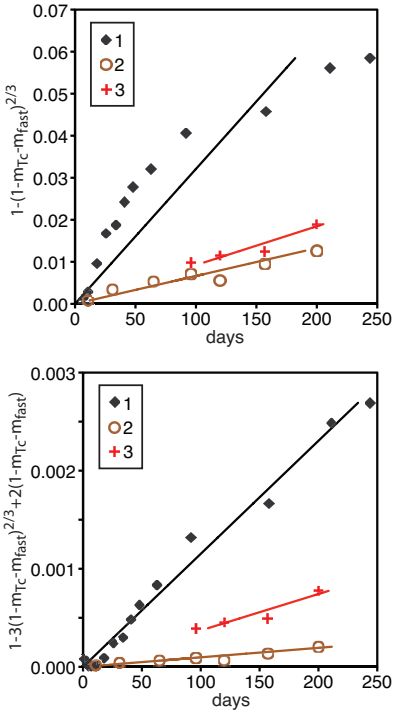

Figure 4. Loss of Tc from Tc-doped iron oxides **1-3** modeled using a dissolving particle model (top) and a diffusion model (bottom) The lines indicate the fit to the data by eqs 2 (top) and 3 (bottom).

In contrast to the relatively rapid release of ^{99}Tc from **1-3** estimated by modeling Tc leaching, nuclear waste glass will retain radionuclides for much longer periods of time due to its much smaller specific surface area. For example, using the bulk density of Fe_3O_4, the crystallite size from XRD, and assuming spherical particles, **1** has a specific surface area of approximately 16 $m^2\ g^{-1}$, while bulk glass has a specific surface area of approximately 0.0001 $m^2\ g^{-1}$ (1 $cm^2\ g^{-1}$) – 5 orders of magnitude smaller. Although the normalized release rate of ^{99}Tc from **1** is about an order of magnitude smaller than that of nuclear waste glass, the fact that the specific surface area of nuclear waste glass is ~5 orders of magnitude smaller than that of **1** makes glass a much better waste form. To convert **1-3** into effective nuclear waste form would require additional processing, such has hot isostatic pressing, to reduce their specific surface areas and consolidate them into a dense, nonporous waste forms.

The most interesting result of the leaching experiments is the leaching behavior of **1** (Tc-doped Fe_3O_4), which strongly suggests that the main pathway for Tc leaching from **1** is solid-state diffusion of Tc(IV) to the surface of the Fe_3O_4 particles. Solid state diffusion of cations, especially Fe(II), in Fe_3O_4 is well-known and is the primary mechanism by which small Fe_3O_4 crystals are oxidized to maghemite (γ-Fe_2O_3).[89-91] Moreover, Ti-doped Fe_3O_4, which is a useful model for Tc-doped Fe_3O_4, shows more rapid loss of Fe(II) relative to Fe_3O_4.[92] The recent observation that Tc(IV) is incorporated into Fe_3O_4 upon immersion of Fe_3O_4 in a pertechnetate solution is consistent with Tc(IV) diffusion into Fe_3O_4 following reduction of TcO_4^- at the surface.[34, 35]

Solid state diffusion is believed to play a role in the release of radionuclides from waste glass; however, this is not the primary pathway for release.[86, 87, 93-96] Waste glass is not thermodynamically stable under environmental conditions and slowly alters to form more stable minerals. This alteration process is the primary pathway for release of radionuclides from waste glasses. On the other hand, most proposed ceramic waste forms are thermodynamically stable and do not form other mineral phases upon aging.[97] For such materials, the primary radionuclide release pathways are solid state diffusion and dissolution/reprecipitation (analogous to Ostwald ripening). The ^{99}Tc leach rates from Tc-doped iron oxides and anatase (TiO_2) can be compared with the known dissolution rates of iron oxides and rutile (TiO_2) to examine whether the trend in Tc leach rates (Fe_3O_4 > $MgFe_2O_3$ ~ α-Fe_2O_3 >> TiO_2) is consistent with Tc release via dissolution/reprecipitation. The dissolution rates of both hematite and rutile are first order in [H^+], so the dissolution rates determined in acid may be converted to the dissolution rates at the pH in the leaching solutions (Table 3).[98, 99] As shown in Table 3, the trend in dissolution rates of the oxide phases (TiO_2 >> α-Fe_2O_3 ~ Fe_3O_4 >> $MgFe_2O_4$) is not consistent with the observed Tc leach rates.

Table 3. Leach rates of Tc-doped oxides and dissolution rates of the oxide matrices

	NL(^{99}Tc) (g m^{-2} d^{-1})	pH after leaching	Oxide dissolution rate at leaching pH (mol m^{-2} d^{-1})
1 (Tc in Fe_3O_4)	4×10^{-5}	7.2	1.9×10^{-11}
2 (Tc in $MgFe_2O_4$)	2×10^{-5}	7.1	7.1×10^{-13}[a]
3 (Tc in α-Fe_2O_3)	2×10^{-5}	4.1	8.9×10^{-10}
Tc in TiO_2 [59]	3×10^{-6}	4.2	1.1×10^{-8}

a) Dissolution rate of $MgFe_2O_4$ assumed to be identical to that of γ-Fe_2O_3

The alternative explanation for the trend in leach rates is differences in solid state diffusion.[89] While solid state diffusion rates are known at high temperature for the host oxide phases, they have not been reported near ambient temperatures. Solid state diffusion rates are heavily dependent on the concentration of defects since the lowest energy diffusion mechanism occurs via an atom migrating to a defect site. Among the materials examined here, **1** has the highest concentration of defects, especially vacancies, due to maghematization, and Tc doped TiO_2 is expected to have the lowest concentration of defects because replacing Ti(IV) by Tc(IV) is charge neutral. Simply doping the iron oxides with Tc(IV) greatly increases the potential for formation of vacancies. These defects are well known in spinels, and their presence has been suggested in hematite doped with Sn(IV) or Ti(IV).[100] In addition to the defects created by doping Tc(IV) into these oxides, radiation damage creates defects as the radionuclides decay.[101]

Conclusions

The goals of this work were to prepare Tc-doped iron oxides in aqueous solution starting from TcO_4^- in nitric acid and to determine the Tc release rates of the resulting materials. The Tc doped iron oxides may be prepared by first chemically denitrating the nitric acid solution using formic acid, which produces TcO_4^- in a mixture of dilute nitric and formic acids. Ferrous nitrate was formed *in situ* by dissolution of iron powder. Neutralization of this solution with NH_4OH followed by heating at reflux for 1 hour yields Tc-doped Fe_3O_4 and heating at reflux for 18 hours produces Tc-doped α-Fe_2O_3. Tc-doped $MgFe_2O_4$ was produced by adding $Mg(OH)_2$ to the $Fe(NO_3)_2$ solution prior to neutralization with NH_4OH followed by heating at reflux for 1 hour. The local structures of Tc in these materials were determined by Tc K-edge EXAFS and are consistent with Tc replacing Fe(III) on octahedral

sites in the iron oxide phase identified by XRD. The Tc-doped iron oxide nanoparticles were leached with DI water and the normalized release rates of Tc were found to vary from 4×10^{-5} g m^{-2} d^{-1} to 1×10^{-4} g m^{-2} d^{-1}. These normalized release rates are an order of magnitude slower than the normalized release rate of boron from nuclear waste glass (boron has the same release rate as Tc). These results suggest that iron oxides, especially $MgFe_2O_4$ and α-Fe_2O_3, are potentially useful matrices for immobilizing Tc. However, due to their small particle sizes, none of the materials produced in this study are effective nuclear waste forms without further processing. As previously noted for Tc-doped TiO_2, Tc-doped iron oxides would need to be consolidated into a dense form, either by hot pressing or pressing and sintering, to produce an effective waste form for ^{99}Tc. Modeling the release of Tc from Fe_3O_4 and comparison of the Tc leach rates from iron and titanium oxides suggests that Tc leaching is controlled by solid state diffusion.

Conflicts of interest

There are no conflicts to declare.

Acknowledgements

This work was supported by the U.S. Department of Energy, Office of Science, Basic Energy Sciences, Chemical Sciences, Biosciences, and Geosciences Division (CSGB), Heavy Element Chemistry Program and was performed at Lawrence Berkeley National Laboratory under contract No. DE-AC02-05CH11231. Tc K-edge XAFS spectra were obtained at the Stanford Synchrotron Radiation Lightsource, SLAC National Accelerator Laboratory, which is supported by the U.S. Department of Energy, Office of Science, Office of Basic Energy Sciences under Contract No. DE-AC02-76SF00515. Travel to SSRL (SAS) was supported by the DOE Waste Treatment and Immobilization Plant Project of the Office of River Protection. PNNL is operated for the DOE by Battelle Memorial Institute under Contract DEAC05-76RL01830.

Notes and references

1. J. P. Icenhower, N. P. Qafoku, J. M. Zachara and W. J. Martin, *Am. J. Sci.*, 2010, **310**, 721-752.
2. N. J. Pilkington, *J. Less Common Met.* , 1990, **161**, 203-212.
3. S. Kunze, V. Neck, K. Gompper and T. Fanghanel, *Radiochim. Acta*, 1996, **74**, 159-163.
4. T. Ishii and T. Sakuragi, *Radioisotopes*, 2006, **55**, 485-494.
5. L. C. Hebel, E. L. Christensen, F. E. Donath, W. E. Falconer, L. J. Lidofsky, E. J. Moniz, T. H. Moss, R. L. Pigford, T. H. Pigford, G. I. Rochlin, R. H. Silsbee, W. M.E., H. Frauenfelder, T. L. Cairns, W. K. H. Panofsky and M. G. Simmons, *Rev. Mod. Phys.*, 1978, **50**, S1-S185.
6. *Yucca Mountain Repository License Application*, U.S. Department of Energy, 2008.
7. F. M. Mann, R. J. Puigh, S. H. Finfrock, R. Khaleel and M. I. Wood, *Integrated Disposal Facility Risk Assessment*, CH2M Hill Hanford Group, Inc., Richland, WA, 2003.
8. *Performance Assessment for the Saltstone Disposal Facility at the Savannah River Site*, SRR Closure & Waste Disposal Authority, Aiken, SC, 2009.
9. *EPA facts about Technetium-99*, U.S. Environmental Protection Agency, 2014.
10. D. J. Liu, J. Yao, B. Wang, C. Bruggeman and N. Maes, *Radiochim. Acta*, 2007, **95**, 523-528.
11. N. J. Hess, Y. X. Xia, D. Rai and S. D. Conradson, *J. Solution Chem.*, 2004, **33**, 199-226.
12. B. H. Gu, W. M. Dong, L. Y. Liang and N. A. Wall, *Environ. Sci. Technol.*, 2011, **45**, 4771-4777.
13. M. A. Boggs, T. Minton, W. M. Dong, S. Lomasney, M. R. Islam, B. H. Gu and N. A. Wall, *Environ. Sci. Technol.*, 2011, **45**, 2718-2724.
14. T. Sekine, A. Watanabe, K. Yoshihara and J. I. Kim, *Radiochim. Acta*, 1993, **63**, 87-90.
15. W. W. Lukens, D. A. McKeown, A. C. Buechele, I. S. Muller, D. K. Shuh and I. L. Pegg, *Chem. Mater.*, 2007, **19**, 559-566.
16. H. Migge, *Mater. Res. Soc. Symp. Proc.*, 1990, **176**, 411-417.
17. H. Lammertz, E. Merz and S. Halaszovich, *Mater. Res. Soc. Symp. Proc.*, 1985, **44**, 823-829.
18. N. E. Bibler, T. L. Fellinger, S. L. Marra, R. J. O'Driscoll, J. W. Ray and W. T. Boyce, *Mater. Res. Soc. Symp. Proc.*, 2000, **608**, 697-702.
19. M.-S. Lee, W. Um, G. Wang, A. A. Kruger, W. W. Lukens, R. Rousseau and V.-A. Glezakou, *Nature Commun.*, 2016, **7**, 12067.
20. D.-S. Kim and A. A. Kruger, *J. Non-Cryst. Sol.*, 2017, **in press**.

21. B. Grambow, *Elements*, 2006, **2**, 357-364.
22. A. E. Ringwood, S. E. Kesson, N. G. Ware, W. Hibberson and A. Major, *Nature*, 1979, **278**, 219-223.
23. O. Muller, W. B. White and R. Roy, *J. Inorg. Nucl. Chem.*, 1964, **26**, 2075-2086.
24. A. Edouminko, F. Colin and J. J. Trescases, *J. Afr. Earth Sci.*, 1995, **21**, 313-318.
25. E. Ramanaidou, D. Nahon, A. Decarreau and A. J. Melfi, *Clay Clay Miner.*, 1996, **44**, 22-31.
26. D. L. Shuster, P. M. Vasconcelos, J. A. Heim and K. A. Farley, *Geochim. Cosmochim. Acta*, 2005, **69**, 659-673.
27. C. J. Yapp, *Geochim. Cosmochim. Acta*, 2000, **64**, 2009-2025.
28. F. N. Skomurski, K. M. Rosso, K. M. Krupka and B. P. McGrail, *Environ. Sci. Technol.*, 2010, **44**, 5855-5861.
29. X. Guo, R. K. Kukkadapu, A. Lanzirotti, M. Newville, M. H. Engelhard, S. R. Sutton and A. Navrotsky, *Inorg. Chem.*, 2015, **54**, 4156-4166.
30. K. R. Whittle, M. G. Blackford, K. L. Smith, N. J. Zaluzec, M. Weyland and G. R. Lumpkin, *J. Nucl. Mat.*, 2015, **462**, 508-513.
31. R. D. Shannon, *Acta Cryst. A*, 1976, **32**, 751-767.
32. S. A. Luksic, B. J. Riley, M. Schweiger and P. Hrma, *J. Nucl. Mat.*, 2015, **466**, 526-538.
33. S. E. Pepper, D. J. Bunker, N. D. Bryan, F. R. Livens, J. M. Charnock, R. A. D. Pattrick and D. Collison, *J. Colloid Interface Sci.*, 2003, **268**, 408-412.
34. T. Kobayashi, A. C. Scheinost, D. Fellhauer, X. Gaona and M. Altmaier, *Radiochim. Acta*, 2013, **101**, 323-332.
35. E. Yalcintas, A. C. Scheinost, X. Gaona and M. Altmaier, *Dalton Trans.*, 2016, **45**, 17874-17885.
36. T. A. Marshall, K. Morris, G. T. W. Law, J. F. W. Mosselmans, P. Bots, S. A. Parry and S. Shaw, *Environ. Sci. Technol.*, 2014, **48**, 11853-11862.
37. F. N. Smith, W. Um, C. D. Taylor, D.-S. Kim, M. J. Schweiger and A. A. Kruger, *Environ. Sci. Technol.*, 2017, **50**, 5216-5224.
38. S. A. Saslow, W. Um, C. I. Pearce, M. H. Engelhard, M. E. Bowden, W. W. Lukens, I. I. Leavey, B. J. Riley, D.-S. Kim, M. J. Schweiger and A. A. Kruger, *Environ. Sci. Technol.*, 2017, **51**, 8635-8642.
39. W. Um, H. Chang, J. P. Icenhower, W. W. Lukens, R. J. Serne, N. Qafoku, R. K. Kukkadapu and J. H. Westsik, *J. Nucl. Mat.*, 2012, **429**, 201-209.
40. W. Um, H. S. Chang, J. P. Icenhower, W. W. Lukens, R. J. Serne, N. P. Qafoku, J. H. Westsik, E. C. Buck and S. C. Smith, *Environ. Sci. Technol.*, 2011, **45**, 4904-4913.
41. F. N. Smith, C. D. Taylor, W. Um and A. A. Kruger, *Env. Sci. Technol.*, 2017, **49**, 13699-13707.
42. B. F. Bohor, E. E. Foord and R. Ganapathy, *Earth Planet. Sci. Lett.*, 1986, **81**, 57-66.
43. F. T. Kyte and J. A. Bostwick, *Earth Planet. Sci. Lett.*, 1995, **132**, 113-127.
44. K. Righter and R. T. Downs, *Meteorit. Planet. Sci.*, 2000, **35**, A136-A137.
45. H. Causevic, H. Morras, A. Mijovilovich and C. Saragovi, *Physica B Condens. Matter.*, 2004, **354**, 373-376.
46. H. S. C. O'Neill, H. Annersten and D. Virgo, *Am. Mineral.*, 1992, **77**, 725-740.
47. Z. X. Tang, C. M. Sorensen, K. J. Klabunde and G. C. Hadjipanayis, *J. Colloid. Interface. Sci.*, 1991, **146**, 38-52.
48. T. Kodama, Y. Wada, T. Yamamoto, M. Tsuji and Y. Tamaura, *J. Mater. Chem.*, 1995, **5**, 1413-1418.
49. T. Sugimoto and E. Matijevic, *J. Colloid Interface Sci.*, 1980, **74**, 227-243.
50. K. Kaneko and T. Katsura, *Bull. Chem. Soc. Jpn.*, 1979, **52**, 747-752.
51. A. Lopez-Delgado, F. A. Lopez, J. L. M. de Vidales and E. Vila, *J. Mater. Res.*, 1999, **14**, 3427-3432.
52. T. Kanzaki, J. Nakajima, Y. Tamaura and T. Katsura, *Bull. Chem. Soc. Jpn.*, 1981, **54**, 135-137.
53. M. Kiyama, *Bull. Chem. Soc. Jpn.*, 1978, **51**, 134-138.
54. W. W. Lukens, N. Magnani, T. Tyliszczak, C. I. Pearce and D. K. Shuh, *Environ. Sci. Technol.*, 2016, **50**, 13160-13168.
55. G. F. Vandegrift, M. C. Regalbuto, S. Aase, A. Bakel, T. J. Battisti, D. Bowers, J. P. Byrnes, M. A. Clark, D. G. Cummings, J. W. Emery, J. R. Falkenberg, A. V. Gelis, C. Pereira, L. Hafenrichter, Y. Tsai, K. J. Quigley and M. H. Van der Pol, presented in part at the ATALANTE 2004: Advances for Future Nuclear Fuel Cycles, Nimes, France, 2004.
56. R. F. Bradley and C. B. Goodlett, *Denitration of Nitric Acid Solution by Formic Acid*, Savannah River Laboratory, Aiken, SC, 1972.
57. J. M. McKibben, *Radiochim. Acta*, 1984, **36**, 3-15.
58. *U.S.A Pat.,* U.S. 2009/0298681 A1, 2009.
59. W. W. Lukens and S. A. Saslow, *Chem. Mater.*, 2017, **29**, 10369-10376.
60. D. S. Hwang, E. H. Lee, K. W. Kim, K. I. Lee, J. H. Park, J. H. Yoo and S. J. Park, *J. Ind. Eng. Chem.*, 1999, **5**, 45-51.
61. T. Degen, M. Sadki, E. Bron, U. König and G. Nénert, *Powder Diffr.*, 2014, **29**, S13-S18.
62. D. C. Koningsberger and R. Prins, *X-Ray Absorption: Principles, Applications, Techniques of EXAFS, SEXAFS, and XANES*, John Wiley & Sons, New York, 1988.
63. M. Newville, *J. Synchrotron Rad.*, 2001, **8**, 322-324.
64. B. Ravel, *Phys. Scripta*, 2005, **T115**, 1007-1010.
65. J. Mustre de Leon, J. J. Rehr, S. I. Zabinsky and R. C. Albers, *Phys. Rev. B*, 1991, **44**, 4146-4156.
66. F. Bosi, U. Halenius and H. Skogby, *Am. Mineral.*, 2009, **94**, 181-189.

67. L. Downward, C. H. Booth, W. W. Lukens and F. Bridges, *AIP Conf. Proc.*, 2007, **882**, 129.
68. G. K. Das, S. Acharya, S. Anand and R. P. Das, *Min. Process. Extr. Metall. Rev.*, 1996, **16**, 185-210.
69. D. Calla-Choque, F. Nava-Alonso and J. C. Fuentes-Aceituno, *J. Hazard. Mat.*, 2016, **317**, 440-448.
70. J. Babčan, *Geol. Carpath.* , 1971, **22**, 299-304.
71. B. A. Wechsler, D. H. Lindsley and C. T. Prewitt, *Am. Mineral.*, 1984, **69**, 754-770.
72. A. Cervellino, R. Frison, G. Cernuto, A. Guagliardi and N. Masciocchi, *J. Appl. Crystallogr.*, 2014, **47**, 1755-1761.
73. C. J. Goss, *Phys. Chem. Minerals*, 1988, **16**, 164-171.
74. E. N. Maslen, V. A. Streltsov, N. R. Streltsova and N. Ishizawa, *Acta Crystallogr. Sect. B-Struct. Commun.*, 1994, **50**, 435-441.
75. A. Stefansson, *Environ. Sci. Technol.*, 2007, **41**, 6117-6123.
76. K. E. Linder, J. C. Dewan and A. Davison, *Inorg. Chem.*, 1989, **28**, 3820-3825.
77. G. Anderegg, E. Muller and K. Zollinger, *Helv. Chim. Acta*, 1983, **66**, 1593-1598.
78. R. Alberto and G. Anderegg, *Inorg. Chim. Acta*, 1990, **178**, 125-130.
79. H. B. Burgi, G. Anderegg and P. Bauenstein, *Inorg. Chem.*, 1981, **20**, 3829-3834.
80. J. Campbell, C. Hoenig, F. Bazan, F. Ryerson, M. Guinan, R. Van Konynenburg and R. Rozsa, *Properties of SYNROC-D Nuclear Waste Form: A State-of-the-Art Review*, Lawrence Livermore National Laboratory, Livermore, CA, 1982.
81. W. L. Ebert, S. F. Wolf and J. K. Bates, *Mater. Res. Soc. Symp. Proc.*, 1996, **412**, 221-227.
82. N. E. Bibler and A. R. Jurgensen, *Mater. Res. Soc. Symp. Proc.*, 1988, **112**, 585-593.
83. S. Rolland, M. Tribet, C. Jegou, V. Broudic, M. Magnin, S. Peuget, T. Wiss, A. Janssen, A. Blondel and P. Toulhoat, *Int. J. Appl. Glass Sci.*, 2013, **4**, 295-306.
84. J. H. Westsik, C. O. Harvey and W. L. Kuhn, *High-Temperature Leaching of an Actinide-Bearing, Simulated High-Level Waste Glass*, Pacific Northwest Laboratory, 1983.
85. A. E. Ringwood, *Mineral. Mag.*, 1985, **49**, 159-176.
86. J. K. Bates, C. R. Bradley, E. C. Buck, J. C. Cunnane, W. L. Ebert, X. Feng, J. J. Mazer, D. J. Wronkiewicz, J. Sproull, W. L. Bourcier, B. P. McGrail and M. K. Altenhofen, *High-Level Waste Borosilicate Glass: A Compendium of Corrosion Characteristics, Volume 2*, United States Department of Energy, Office of Waste Management, 1994.
87. A. Barkatt, B. C. Gibson, P. B. Macedo, C. J. Montrose, W. Sousanpour, A. Barkatt, M.-A. Boroomand, V. Rogers and M. Penafiel, *Nucl. Tech.*, 1985, **72**, 140-164.
88. P. Levenspiel, *Chemical Reaction Engineering, Third Edition*, John Wiley & Sons, New York, 1999.
89. J. A. Van Orman and K. L. Crispin, *Rev. Mineral. Geochem.*, 2010, **72**, 757-825.
90. K. J. Gallagher, W. Feitknecht and U. Mannweiler, *Nature*, 1968, **217**, 1118-1121.
91. J. Tang, K. A. Bosnick and L. E. Brus, *J. Phys. Chem. B*, 2003, **107**, 7501-7506.
92. C. I. Pearce, O. Qafoku, J. Liu, E. Arenholz, S. M. Heald, R. K. Kukkadapu, C. A. Gorski, C. M. B. Henderson and K. M. Rosso, *J. Colloid Interface Sci.*, 2012, **387**, 24-38.
93. H. Matzke and E. Vernaz, *J. Nucl. Mat.*, 1993, **201**, 295-309.
94. J. J. Neeway, S. N. Kerisit, J. Liu, J. Zhang, Z. Zhu, B. J. Riley and J. V. Ryan, *J. Phys. Chem. C*, 2016, **120**, 9374-9384.
95. K. Ferrand, A. Abdelouas and B. Grambow, *J. Nucl. Mat.*, 2006, **355**, 54-67.
96. T. Chave, P. Frugier, A. Ayral and S. Gin, *J. Nucl. Mat.*, 2007, **362**, 466-473.
97. A. G. Solomah and L. R. Zumwalt, *Nucl. Chem. Waste Man.*, 1982, **3**, 111-116.
98. A. A. Baba, F. A. Adekola, E. E. Toye and R. B. Bale, *J. Miner. Mater. Charact. Eng.*, 2009, **8**, 787-801.
99. P. S. Sidhu, R. J. Gilkes, R. M. Cornell, A. M. Posner and J. P. Quirk, *Clay Clay Min.*, 1981, **29**, 269-276.
100. F. J. Berry, C. Greaves, O. Helgason, J. McManus, H. M. Palmer and R. T. Williams, *J. Solid State Chem.*, 2000, **151**, 157-162.
101. R. C. Ewing, *Mineral. Mag.*, 2011, **75**, 2359-2377.